MoS$_2$ Nanoplatelet Fillers for Enhancement of the Properties of Waterborne Pressure-Sensitive Adhesives

Vesna Daniloska,[†] Joseph L. Keddie,[‡] José M. Asua,[†] and Radmila Tomovska*[†,§]

[†]POLYMAT and Departamento de Química Aplicada, Facultad de Ciencias Químicas, University of the Basque Country UPV/EHU, Joxe Mari Korta zentroa, Tolosa Hiribidea 72, Donostia-San Sebastián 20018, Spain

[§]IKERBASQUE, Basque Foundation for Science, Maria Diaz de Haro 3, Bilbao 48013, Spain

[‡]Department of Physics and Surrey Materials Institute, University of Surrey, Guildford, Surrey GU2 7XH, United Kingdom

Ⓢ Supporting Information

ABSTRACT: Nanocomposite pressure-sensitive adhesives (PSAs) composed of polyurethane (PU)/(meth)acrylates reinforced with MoS$_2$ nanoplatelets were prepared by blending aqueous dispersions. MoS$_2$ crystals were exfoliated by sonication in water in the presence of poly(vinylpyrrolidone) (PVP, molecular weight of 10 000 g mol^{-1}) to prepare an aqueous dispersion. Waterborne colloidal polymer particles (latex) were synthesized by miniemulsion photopolymerization in a continuous tubular reactor. The adhesive and mechanical properties from the resulting nanocomposite films were determined as the MoS$_2$ fraction was increased. A superior balance of viscoelastic properties was achieved with 0.25 wt % loading of the MoS$_2$ nanoplatelets, leading to a tack adhesion energy that was three times greater than that for the original PSA.
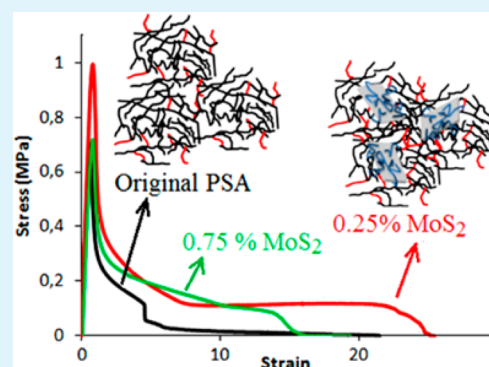
1. INTRODUCTION

Interest in polymer nanocomposites was first stimulated by the reports of Toyota scientists about the advantages of mixing inorganic nanoparticles with polymers, leading to a new direction in the field of materials science.[1] The use of inorganic nanoparticles with different shapes (e.g, platelets, spheres, or tubes) as fillers in a polymer matrix has attracted increasing interest owing to the attractive properties arising from their small size and large aspect ratios, with applications in structural engineering and drug delivery, etc.[2,3] These polymer nanocomposites can be produced by different methods such as in situ polymerization,[4,5] where the polymerization is performed in the presence of nanoparticles; melt blending,[6−8] where a polymer is blended with nanoparticles and then annealed at a temperature above the glass transition temperature of the polymer to form the nanocomposite; or solution blending,[9−11] where the blending of polymer and nanoparticles is performed in a suitable solvent. For the production of waterborne nanocomposites for application as paints, coatings, and adhesives, two main methods have been reported: (1) emulsion mixing and (2) in situ polymerization in suspension,[12] emulsion,[13−16] and miniemulsion.[17−21] The emulsion mixing method has shown to be the most simple and most effective method, as it consists of a simple blending of an aqueous dispersion of nanoparticles with the latex.[14,22−24] One advantage of this simple method is that the polymer properties can be controlled during their synthesis and not perturbed by the presence of nanoparticles. A second advantage is that

mixing at the nanoscale can be achieved, and the larger polymer particles can be used to organize or direct the position of the inorganic nanoparticles.

One of the promising applications of polymer nanocomposites is in pressure-sensitive adhesives (PSAs).[22−26] The adhesive properties of PSAs result from their well-balanced viscoelasticity in which there is viscous dissipation combined with sufficient elasticity.[25,27] The viscous component ensures good wetting of the substrate and enables extension during debonding; the solid component resists deformation and supports load under shear stress. The utilization of various inorganic nanoparticles has provided a promising alternative[19,22,23,28] to the classical polymer−polymer hybrids.[29,30] Reports of different nanoparticles used for preparation of waterborne PSAs nanocomposites (e.g., clay discs (laponite or montmorillonite), carbon nanotubes (multiwalled MWNTs or single-walled SWNT), and graphene) can be found in both the open and patent literature.[15,19,22−24]

Improved adhesive properties have been obtained by the use of plate-like fillers, which are of interest in the present work. Crucially, rearrangement of hard particles in a viscous matrix and the sliding of a viscous matrix along the hard particle surface can both dissipate energy during the deformation of the nanocomposite. It is known that mechanisms of energy

dissipation increase tack adhesion of PSAs. As nanoparticles have a very high surface area, interfacial interactions (such as adsorption of polymer chains and sliding along interfaces) can make a significant impact on a soft matrix. For instance, laponite armored poly(lauryl acrylate) nanoparticles showed a significant enhancement of the tack energy as compared with unarmored latexes.[28] Khan et al.[31] added graphene sheets to a poly(vinyl acetate) adhesive and reported increased adhesion properties.

Inspired by the unique properties of this new class of materials (two-dimensional (2D) one or few molecular layers thin materials) and encouraged by the possibilities of the platelet-like nanoparticles to enhance the adhesive properties, in this study we have used molybdenum disulfide (MoS_2) 2D nanoplatelets as a reinforcing filler in polyurethane (PU)/(meth)acrylate waterborne PSAs. Bulk MoS_2 has a layered structure, with each layer consisting of a covalently bonded S–Mo–S hexagonal quasi two-dimensional network[32,33] and connected to other layers by weak attractive van der Waals forces. Owing to the relatively weak interlayer interaction, the monolayers of MoS_2 can be mechanically exfoliated from a MoS_2 crystal.[34] The literature reports several investigations in which fullerene-like particles of MoS_2 were used as fillers in a polymer matrix to improve the tribological properties[35,36] and thermal stability[37] of the polymer. MoS_2 nanotubes were incorporated into a polyurea elastomer matrix in order to study the influence of the nanotubes on the glass transition temperature.[38] To the best of the authors' knowledge, no work on MoS_2 nanoplatelets in waterborne PSAs has been reported. In this work, for the first time, nanocomposites were prepared by blending exfoliated MoS_2 nanoplatelets in water in the presence of PVP as a dispersant with waterborne PU/(meth)acrylic PSAs. The viscoelastic and adhesive properties with various amounts of MoS_2 filler were investigated. It was demonstrated that the loading of 0.25 wt % nanoplatelets in the soft polymer matrix results in balanced viscoelastic properties and can raise the adhesion energy by about a factor of 3.

2. EXPERIMENTAL SECTION

2.1. Materials. Technical-grade monomers 2-ethylhexyl acrylate (2EHA, Quimidroga), methyl methacrylate (MMA, Quimidroga), methacrylic acid (MAA, Aldrich), and 2-hydroxyethyl methacrylate (HEMA, Fluka) were used as received. N-octadecyl acrylate (SA, Aldrich) was used as a reactive costabilizer in order to prevent Ostwald ripening.[39,40] An aliphatic isocyanate terminated polyurethane (PU) prepolymer, Incorez 701 (Incorez Ltd.) specially designed for adhesive applications, was used without further purification. The equivalent weight of the prepolymer is 1050 g/equivalent. Dibutyltindilaurate (DBTDL) (Aldrich) was used as catalyst for the polyaddition reactions. Dowfax 2A1 (alkyl diphenyloxidedisulfonate, Dow Chemicals) was used as surfactant to prepare the miniemulsions, and sodium dodecyl sulfate (SDS, Aldrich) was added after the miniemulsification to improve the miniemulsion stability. Both were used as received. A nonbleaching, oil-soluble photoinitiator 1-hydroxycyclohexyl phenyl ketone (HCPK, Aldrich) was used as received. Sodium bicarbonate ($NaHCO_3$, Aldrich) was used as a buffer. Gel-permeation-chromatography grade tetrahydrofuran (THF, Scharlau) was used as a solvent. Molybdenum(IV) sulfide (MoS_2) powder was used as received. Three different samples of poly(vinylpyrrolidone) (PVP), with three different weight-average molecular weights (10 000 (PVP10), 55 000 (PVP55), and 360 000 (PVP360) g/mol) (Aldrich), were used as a dispersant for the exfoliation of MoS_2 nanosheets. Oxygen-free grade nitrogen was used for purging the feed. Double deionized (DDI) water was used throughout the work.

2.2. Synthesis of the PU/Acrylic Hybrid Latex. Miniemulsions of 45 wt % solids content were prepared via the formulation shown in Table 1. First, the organic phase containing the photoinitiator HCPK

**Table 1. Formulation Used for Synthesis of the Polyurethane/(Meth)Acrylic Miniemulsion Latex**

component	amount (g)	weight %
2EHA	196.43	91.5[a]
SA	12.5	5.8[a]
MMA	3.04	1.4[a]
MAA	2.03	0.9[a]
HEMA	1.01	0.4[a]
PU	22.5	10[b]
DBTDL	0.11	500 ppm[c]
HCPK	1.01	0.48[a]
DDI water	270.05	
Dowfax 2A1	9	2 (45 wt % active)[b]
NaHCO₃	0.46	0.02 M[d]
SDS	2.25	1[b,e]

[a]Weight based on monomer weight. [b]Weight based on organic weight. [c]Concentration in ppm based on organic phase. [d]Based on water phase. [e]Post miniemulsification addition.

was prepared by dissolving Incorez 701 in the monomer mixture (2EHA/SA/MMA/MAA/HEMA). The organic phase was then mixed with an aqueous solution of the surfactant (Dowfax 2A1) and $NaHCO_3$ under intensive magnetic stirring (15 min at 1000 rpm) to create an emulsion. The resulting coarse emulsion was sonicated in an ice bath for 15 min at 9 output control and 80% duty cycle with a Branson 450 sonicator (Danbury, CT). The temperature after sonication was around 68 °C. Finally, to improve the miniemulsion stability, SDS was added. After the addition, the miniemulsion was cooled to room temperature under agitation (approximately 2 h).

The photopolymerizations were performed at room temperature in a continuous tubular reactor.[41,42] The reactor consisted of a 740-mm silicone tube (2-mm inner diameter) and seven quartz tubes connected to each other with six semicircular silicone bends (2-mm inner diameter). Each quartz tube had a length of 400 mm, an inner diameter of 1 mm, and an outer diameter of 3 mm. It has been shown that this reactor design allows a smooth operation at high solids content avoiding clogging.[43] A UV chamber (model BS 03, Dr. Gröbel UV-Elektronik GmbH) equipped with 20 UV lamps emitting UV light in the range from 315 to 400 nm with a maximum at 368 nm was used. The incident light irradiance was measured using a radiometer UV sensor. A gear pump (model 305, Gilson) was used to feed the miniemulsion (which was kept under stirring at 450 rpm) to the reactor with a flow rate corresponding to a residence time of 10 min, which was enough to achieve almost complete conversion of the acrylic monomers at the reactor outlet.[41,42] Prior to being fed to the reactor, the miniemulsion was purged with nitrogen for about 30 min. The latexes were reacted under steady-state conditions. The reaction temperature was measured at the inlet and at the outlet of the reactor to be 25 °C ± 1 °C in both places. This shows that the reactor efficiently removed the heat of polymerization. Without UV irradiation, no polymerization of the (meth)acrylates took place even in the presence of the initiator. Moreover, direct irradiation of the monomer without a photoinitiator did not lead to the formation of a polymer.

The latex was prepared using incident light irradiance of 7 mW/cm² and PI concentration of 0.48 wt %. The hybrid PU-acrylic polymer is formed through a complex mechanism that has been studied elsewhere.[42,44,45] Here, it is sufficient to say that during the preparation of the miniemulsion, reaction of the isocyanate-terminated PU prepolymer with water and HEMA led to extended and double bond/isocyanate terminated PU. In the reactor, due to the low temperature used (25 °C) and the short residence time (10 min) only free radical polymerization occurred, and the remaining isocyanate
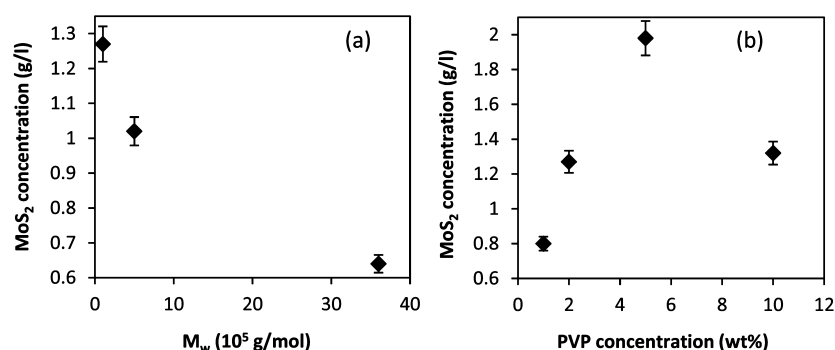
Figure 1. Concentration of exfoliated MoS_2 dispersed in water as a function of (a) the molecular weight of the PVP dispersant (at a constant PVP concentration of 2 wt %, based on MoS_2) and (b) the PVP concentration (with M_w = 10 000 g/mol).

groups reacted during the first 8 days of latex storage.[44] Later, hydrogen bonding and other physical interactions further modified the polymer microstructure.[44] The latex was aged for 230 days to ensure that a stable microstructure was achieved. The average particle size was 150 nm, measured by dynamic light scattering (DLS) (ZetasizerNano Z, Malvern Instruments) and the gel content was 35 wt % according to Soxhlet extraction in THF.

2.3. 2D MoS_2 Nanoplatelets Preparation and Characterization. MoS_2 powder (99.0% purity) with a grain size less than 2 μm was ground in a mortar. The powder was then dispersed in a PVP aqueous solution and was sonicated under stirring for 1 h at a power of 360 W (1 s on and 2 s off) with a tip sonicator Branson 450 (Danbury, CT). The beaker was chilled by immersion in ice–water during sonication. Then the dispersion was centrifuged at 4500 rpm for 30 min. The supernatant containing MoS_2 nanoplatelets was collected. The platelets were observed by transmission electron microscopy (TEM) and atomic force microscopy (AFM) analysis. The TEM images were obtained using a PHILIPS EM208S with a digital camera and a PHILIPS CM120 Biofilter with a STEM module. AFM images were acquired using AFM NTEGRA, NT-MDT in intermittent-contact mode. The nominal resonant frequency of the cantilever (NT-MDT, Moscow, Russia) was 120 kHz and the nominal spring constant was 7 N m^{-1}. Inductively coupled plasma–mass spectrometry (ICP/MS) (ICP/MS Agilent 7700 x) was used to determine the concentrations of MoS_2 nanoplatelets in the supernatant from centrifugation by quantifying the peak at m/z 95, with a calibration of 0, 0.1, 0.25, 0.5, and 1.0 mg L^{-1}, and using an internal standard mix of Bi, Ga, Ge, Rh, and Sc.

2.4. Nanocomposite Preparation. To achieve different MoS_2 concentration with respect to the polymer (from 0.1 to 0.75 wt %), different amounts of the MoS_2 dispersions were added to the PU/(meth)acrylic latexes under stirring. The resulting blends were stable for days; no macroscopic sedimentation of MoS_2 was observed.

2.5. Adhesive, Linear Viscoelastic and Nonlinear Elastic Properties. Probe-tack measurements were performed following the Avery method (MicroSystems Texture Analyzer, Godalming, UK) using a 1-in., spherical stainless steel probe. The films were cast on glass (exactly 1.5 mL of the blend) using a cube applicator (from 200 to 400 μm) and then they were dried for 2 min under irradiation by an IR lamp, followed by 48 h drying at room temperature. The final thickness of the films was calculated from the solids content of the blend used, and the thickness of the films was varied between 60 and 90 μm. The ambient temperature was approximately T = 21 °C and the relative humidity was approximately 40% in all experiments. The procedure for probe-tack tests was as follows: the spherical probe was brought into contact with the film at a velocity of 30 μm s^{-1} and with a load of −4.9 N for 1 s, after which the probe was removed from the film at a controlled velocity that corresponded to an initial debonding rate of 1 s^{-1}. For every sample, the debonding rate was set according to the thickness of the film. The nominal stress is defined as the force divided by the contact area, and the strain is defined as the displacement divided by the thickness of the film. The contact area was calculated after every measurement. For each experiment, five

replicate measurements were made, and the averages are reported here.

Samples for dynamic mechanical analysis (DMA) were obtained by casting the latex in poly(tetrafluoroethylene) molds and drying at room temperature for 7 days. Rectangular samples with approximate dimensions of 10 mm × 3.5 mm × 0.5 mm were cut from the dry films and analyzed using a commercial instrument (Q800, TA Instruments, New Castle, DE, USA) in a tension mode with a strain of 0.25% at a frequency of 1 Hz and a temperature sweep from −80 to 30 °C at a constant heating rate of 4 °C per min.

Stress/strain measurements were carried out on a tensile apparatus (MicroSystems Texture Analyzer, Godalming, UK) with a 5 mm s^{-1} crosshead velocity, which corresponded to an initial strain rate of 1 s^{-1}. For each experiment, four replicate measurements were made, and the averages are reported here.

3. RESULTS AND DISCUSSION

3.1. MoS_2 Exfoliation. The layers in the bulk MoS_2 crystals are connected by weak van der Waals forces. Therefore, to exfoliate the crystal into thin 2D nanoplatelets composed of one or a few molecular layers of covalently bonded S–Mo–S, a low-energy sonication process was used. To hinder restacking of the MoS_2 nanoplatelets, PVP was added as a stabilizing agent prior to the sonication process. After sonication, the dispersions were subjected to centrifugation (4500 rpm, 30 min) in order to remove the MoS_2 that was not exfoliated. Figure 1 presents the effect of the PVP molecular weight and concentration on the concentration of MoS_2 nanoplatelets that remained dispersed in water. It can be seen that for a PVP concentration of 2 wt % (based on MoS_2), the concentration of well dispersed exfoliated nanoplatelets decreased as the molecular weight of the PVP increased (Figure 1a), possibly because there were fewer stabilizing chains when the molecular weight was higher. Because the lowest molecular weight PVP resulted in dispersions with the highest concentrations, it was used in follow-up experiments. Figure 1b shows that the concentration of dispersed nanoplatelets has a maximum for a concentration of 5 wt % PVP (based on MoS_2). With a higher PVP concentration, the stability of the MoS_2 decreased, perhaps because of bridging flocculation. Therefore, for all subsequent experiments, PVP with M_w = 10 000 g/mol and a concentration of 5 wt % was used to disperse the MoS_2. The prepared MoS_2 aqueous dispersions were highly stable during months of storage.

Figure 2 presents the TEM images of the 2D nanoplatelets showing that most of the nanoplatelets were composed of few molecular layers (Figure 2a), but nanoplatelets with a thickness of one or two layers were also observed (Figure 2b). Because of their ultrathin structure, the MoS_2 nanoplatelets are transparent
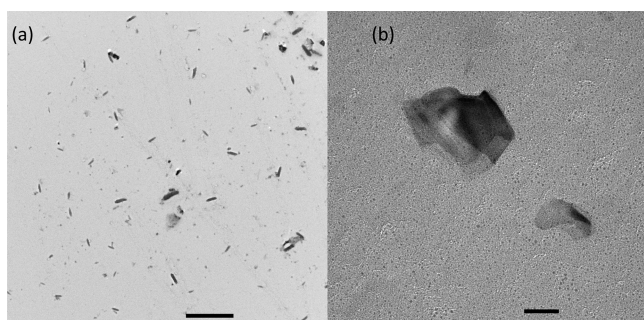
Figure 2. TEM images of exfoliated MoS$_2$ nanoplatelets (a) at low magnification (scale bar = 2 μm) and (b) at higher magnification (scale bar = 50 nm).

to the electron beam. The lateral size of most of the MoS$_2$ nanoplatelets is around 100−300 nm, which is advantageous to facilitate their stabilization in water and blending with latex particles of a similar size. An AFM height image and the cross-sectional traces of MoS$_2$ nanoplatelets spin-casted on mica are presented in Figure 3 confirming the TEM findings. The thickness of the MoS$_2$ nanoplatelets is in the range 2−9 nm, which can be seen from the cross-sectional trace. Bearing in mind that the thickness of a monolayer MoS$_2$ is 0.6 nm[46,47] and the distance between layers is measured to be 0.7 nm,[48] we can conclude that most of the nanoplatelets are composed of between two and four layers of MoS$_2$.

3.2. Adhesive and Mechanical Properties of the Nanocomposite PSAs. The adhesive and mechanical properties (linear viscoelastic and nonlinear elastic properties) of the nanocomposite PSA were determined and compared with the properties of the original PSA. A way to assess the adhesive performance of a PSA is via probe-tack testing in which a probe is brought in to contact with the PSA surface and then removed at a constant velocity. In these experiments, first the probe comes into contact with the adhesive film under a controlled load and set time. When the probe is elevated from an adhesive, a negative pressure is created, which induces the formation of cavities (in a high-performing adhesives). The number of cavities reaches a maximum at maximum stress, σ_{max}. Later, the stress falls to a plateau because of propagation of the cavities laterally and vertically as the walls between the cavities are drawn into fibrils.[49−51] The force that is needed to draw the

fibrils determines the plateau stress, σ_p, at higher strains. Finally, the stress drops to zero when the fibrils break or detach from the probe at maximum strain, ε_f (strain at failure). The area under the stress−strain curve represents the adhesion energy, E_{adh}.

As has been demonstrated in other work,[52,53] the tackiness of adhesive film can be affected by the near-surface composition of the PSAs, which can be influenced by atmospheric conditions (e.g., relative humidity) for some polymer systems with polar chemical groups. To eliminate this influence in the comparison of performance of the films prepared here, all the films were prepared under the same conditions (T = 21 °C and relative humidity of 40%). The tack-probe analyses were carried out under the same conditions (T = 21 °C, relative humidity of 40%) exactly 48 h after casting the film. In this way, the near-surface composition of all investigated films was established under similar conditions and similar aging. Thus, all the identified differences in tackiness can be attributed to the effect of MoS$_2$ nanoplatelets addition.

Figure 4 shows the probe-tack curves of the original PSA (PU/(meth)acrylics) and those of the MoS$_2$ nanocomposite
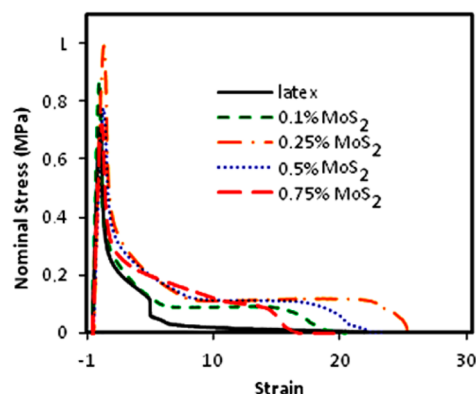
Figure 4. Representative stress−strain curves obtained at room temperature in probe-tack tests on nanocomposite films with different MoS$_2$ concentrations (wt %) indicated in the legend.

PSAs. The probe-tack curve of the original PSA shows a fibrillation plateau that indicates there is some extension of cavities being drawn into fibrils. The abrupt drop in the plateau
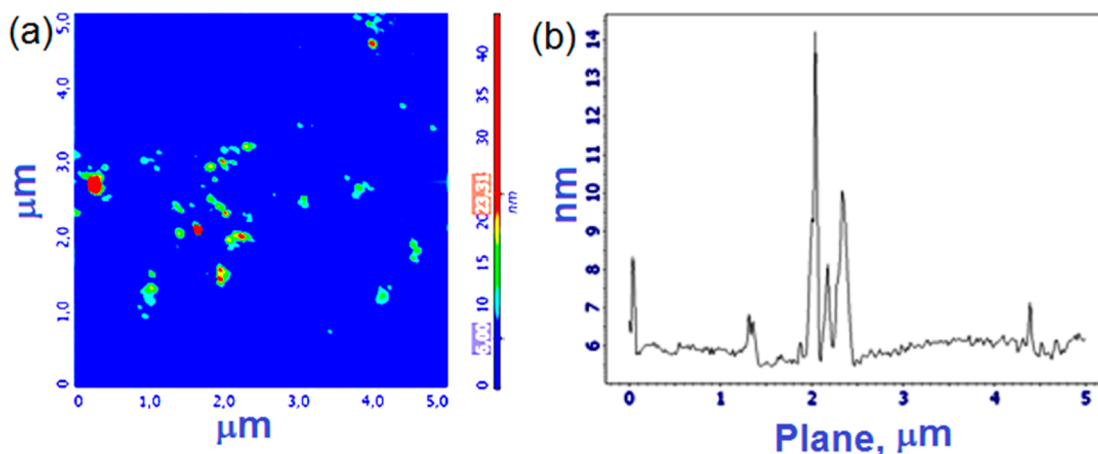
Figure 3. AFM height image (area of 5 μm × 5 μm) (a) and a cross-sectional trace (b) of exfoliated MoS$_2$ spin-cast on mica. The steps in the trace are measurements of the MoS$_2$ platelet thickness.

indicates that the walls of the cavities break and thus reduce the negative pressure. There is a continued extension of the fibrils to higher strains with a low stress level. The gradual decrease in the stress is indicative of cohesive failure, in which the fibrils break because of their low strength. This mechanism was confirmed by the observation of polymer residue on the probe at the end of the test. All nanocomposite PSAs showed extended plateaus on the probe-tack curves, and the curves finally end with a rather abrupt decrease in the force to zero, which indicates an improvement in the cohesive strength. Adding small amounts of MoS_2 nanoplatelets (0.1 wt %) led to a significant extension of the plateau (Figure 4), but there was still cohesive failure. Further increasing of the MoS_2 content in the nanocomposites resulted in a detachment at the interface between the probe and the adhesive layer, via an adhesive (interfacial) debonding mechanism. In this case, no macroscopic residue on the probe at the end of the measurements was observed.

The influence of the MoS_2 nanoplatelets concentration on the work of adhesion (E_{adh}) and the strain at failure (ε_f) is presented in Figure 5. With an increasing concentration of the
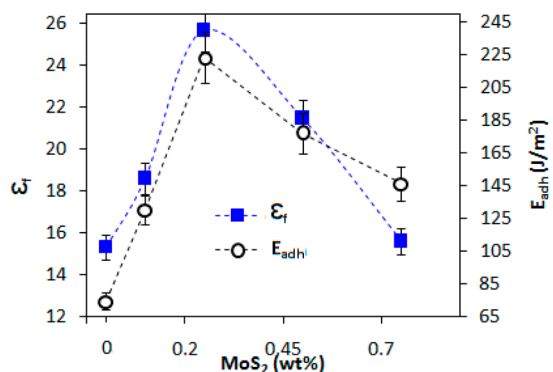
Figure 5. Adhesion energy (E_{adh}) and strain at failure (ε_f) obtained from probe-tack tests at room temperature as a function of MoS_2 concentration in the PSAs. The dashed lines are a guide to the eye.

MoS_2 nanoplatelets, both E_{adh} and ε_f increased and reached their maximum values at a concentrationof 0.25 wt %. Further increasing of MoS_2 in the polymer matrix led to a decrease in both E_{adh} and ε_f (Figure 5).

In an attempt to shed light on the differences observed in the tack adhesion of the nanocomposites, a study of their bulk mechanical properties was carried out. In the design of PSAs, several parameters are important and should be in the optimal range. These parameters include the linear viscoelasticity, which determines whether there is fibrillation or interfacial crack

propagation during debonding and the nonlinear viscoelasticity at high strains, which influences the fibril detachment, whether interfacial (known as adhesive failure) or breaking (known as cohesive failure). High extensibility ensures that the fibrils are strained to high values and hence dissipate a large amount of energy prior to their detachment.

To consider the linear viscoelasticity first, the dynamic moduli are presented. The storage and loss moduli (E' and E'', respectively) as a function of MoS_2 addition are shown in Figure 6. It can be seen (Figure 6a) that there is an increase of the storage modulus of the nanocomposites compared to that of the original polymer, indicating that the introduction of MoS_2 nanoplatelets enhances the stiffness, over the entire temperature range above the polymer's glass transition temperature. The increase in storage modulus with increasing MoS_2 content is clearly seen in the range of higher temperatures (0−25 °C), shown enlarged in the inset figure. The properties in this temperature range determine the PSA performance in the probe-tack tests at room temperature.

The E'' peaks presented in Figure 6b were used to find the polymer's glass transition temperature, T_g. The calculated values are listed in Table 2 and demonstrate that the T_g

Table 2. Glass Transition Temperature (T_g) (Obtained from the E″ Peak) of the Original PU/(meth)acrylic Polymer and the Nanocomposites

MoS_2 content (wt % on polymer)	T_g (°C)
0	−68.8
0.10	−58.8
0.25	−56.9
0.50	−57.8
0.75	−58.9

increases with the addition of the nanoplatelets. The maximum shift of +11.9 °C (Table 2) was found in nanocomposites containing 0.25 wt % MoS_2. The observed increases of the T_g and the storage modulus provide evidence for interactions between the nanoplatelets and the polymer reducing the chain mobility.

In previous studies of nanocomposite adhesives containing MWNTs, observed improvements in mechanical and adhesive properties were strongly linked to the type of the dispersant used. That is, PVP dispersants yielded better properties than poly(vinyl alcohol) and conventional anionic and nonionic surfactants.[23] It was suggested previously that the dispersant acts as a bridge between the dispersed material and the polymer matrix, which implies that the dispersant was anchored to the dispersed material and had physical interactions with the
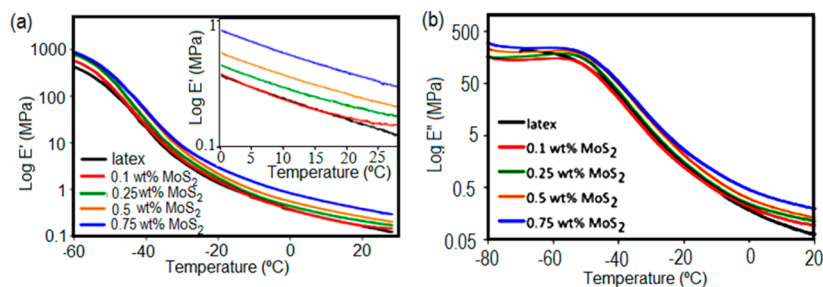
Figure 6. (a) Temperature dependence of the storage, E' (b), and loss, E'', moduli of the original PU/(meth)acrylic PSA and nanocomposite PSAs. The peaks in E'' define the polymer's T_g. The measurements were performed at a heating rate of 4 °C min^{-1} and frequency of 1 Hz.
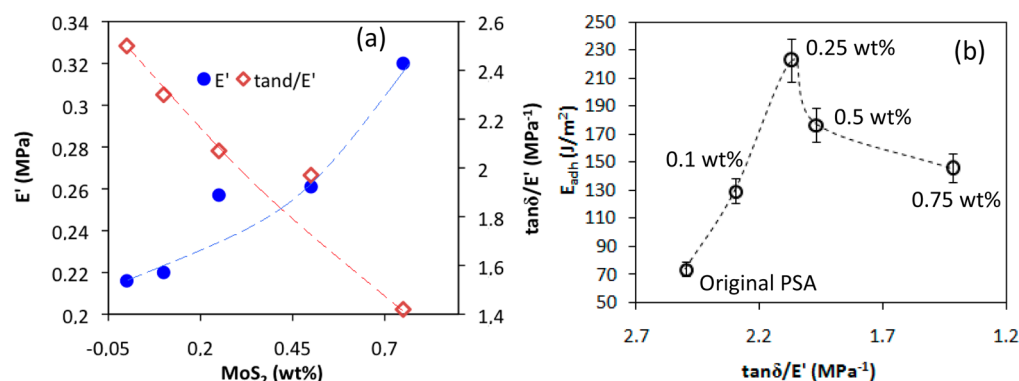
Figure 7. (a) Storage modulus (E') and tan δ/E' as a function of the MoS$_2$ concentration. Measurements were made at a temperature of 25 °C and a frequency of 1 Hz. (b) Adhesion energy (E_{adh}) of PSAs as a function of tan δ/E' for the composite of varying MoS$_2$ concentrations, as indicated. The dashed lines are a guide to the eye.

polymer. For the present case, anchoring of the PVP to the MoS$_2$ may be reinforced by hydrogen bonding of the S atoms of the MoS$_2$ and the PVP chains. Recently, Reinecker et al.[38] demonstrated that the S atoms of MoS$_2$ nanotubes are able to form intermolecular hydrogen bonding with polyurea chains. On the other hand, a necessary condition for the strong interaction between polymers is that they should be compatible. A way of assessing the compatibility between polymers is to check if the Flory–Huggins interaction parameter ($\chi_{PVP-P2EHA}$) is lower than their critical interaction parameter (χ_{cr}). In the Supporting Information it is shown that this is the case for the present system as $\chi_{PVP-P2EHA} = 0.0065$ and $\chi_{cr} = 0.017$. Therefore, the PVP is compatible with the P2EHA in the PSA. The molecular weight of the PVP used (10 000 g mol^{-1}) is lower than its entanglement molecular weight (17 000 g mol^{-1}),[54] therefore entanglements between PVP and P2EHA were not formed. Nevertheless, it has been reported that even molecular weights that are one-half of the entanglement molecular weight can lead to an improvement of the adhesion to hard surfaces.[55] For the present case, the interfacial PVP chains provide to the adhesive an additional energy dissipation mechanism when the MoS$_2$ nanoplatelets slide along the polymer matrix.

Loadings higher than 0.25 wt % led to a decrease of both the adhesive properties and the T_g, perhaps because of the increased aggregation and restacking of the nanoplatelets placed in the small excluded volume between the particles of the hybrid latex dispersion.

The dependence of the E' and tan δ/E' on the MoS$_2$ concentration at a temperature of 25 °C and at a frequency of 1 Hz is presented in Figure 7a. It can be seen that the storage modulus increases with an increasing MoS$_2$ concentration. The storage modulus for all the concentrations used, except for the highest one (0.75 wt %), lies in the range below 0.3 MPa, which according to the Dahlquist criterion[56] is the maximum of the recommended range of E' values for high tack adhesion. (Here the polymer is being described as a noncompressible solid, such that $G' = E'/3$). With a higher E', the force to strain the polymer is greater than the debonding force and interfacial cracking can develop. The high E' value for 0.75 wt % MoS$_2$ explains the poorer tack adhesion properties shown previously in Figures 4 and 5. The tan δ/E' ratio constantly decreases with increasing MoS$_2$ concentration (Figure7a). The high value of tan δ/E' obtained for the original PSA explains the liquid-like behavior of this PSA (fibrillation at high strains previously

shown in tack curves, Figure 4, although the fibrils undergo cohesive failure).

To understand the differences in adhesive properties presented in Figure 4, the dissipative properties of the latex and nanocomposites in relation to their elastic components are next considered. As noted previously, a simple criterion to predict adhesive performance is the ratio tan δ/E'. Values higher than a critical level, which according to Deplace et al.[57] for adhesion on stainless steel is 0.167×10^{-5} Pa^{-1}, favor the development of fibrils rather than interfacial crack propagation. The adhesion energy as a function of the ratio tan δ/E' was plotted in Figure 7b. The original PSA has the highest value for tan δ/E' (Figure 7b), which implies a greater tendency for fibrillation. It can be seen from the probe-tack curve (Figure 4) that the original PSA fibrillates at high strain, however it does not have enough cohesive strength to support the high stress. Consequently, the adhesion energy is low (Figure 7b). When increasing the nanoplatelets concentration, the ratio tan δ/E' decreases and the adhesion energy increases, reaching a maximum at 0.25 wt % nanoplatelets concentration. When there is a decrease in tan δ/E' there is an increase in E_{adh} because cohesive failure is avoided with stronger and extendable fibrils. Below a certain value of the tan δ/E', namely for loadings higher than 0.25 wt %, which in this case is 2.04 MPa^{-1}, the adhesive is too stiff (its modulus is too high) and the adhesive failure occurs at lower strains leading to a decrease in E_{adh}. The adhesion energy of the nanocomposites containing 0.25 wt % MoS$_2$ is 223 J m^{-2}, which is three times higher than found for the original PSA.

The large-strain properties of the nanocomposite PSAs were studied in tensile experiments to aid in the explanation of the PSA debonding in the tack test at large strains. In this regime, a large extensibility is required for a long plateau in the tack curve and a high tack energy. The tensile stress measurements were performed at a strain rate corresponding to that used in the probe-tack measurements. Figure 8 shows that for the original PSA, no strain hardening was observed in the tensile stress–strain curve, which correlates with the liquid-like characteristics found in the probe-tack analysis (Figure 4). The figure also shows that the addition of a small amount of nanoplatelets (0.1 wt %) had a noticeable effect on the stress level at large strains, which can explain the increased cohesion observed in the probe-tack data for this nanocomposite PSA. With 0.1% MoS$_2$ load, the probe-tack data in Figure 4 show that the fibrils are stable when strained to large values, and the stress level of the plateau is raised. Higher MoS$_2$ amounts (>0.25 wt %) gave
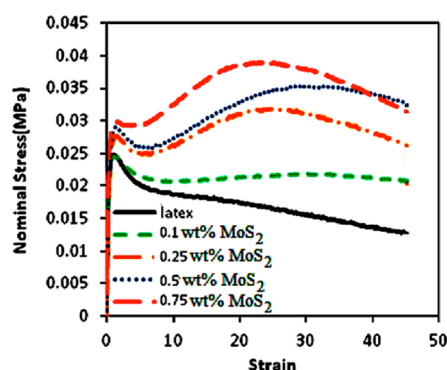
Figure 8. Effect of MoS$_2$ concentration on the tensile stress–strain relations of the nanocomposites at room temperature.

sufficient reinforcement to the nanocomposites to yield strain hardening at high strains. The plateau in the probe-tack analysis extended with increased MoS$_2$ loading, which can be explained by the reinforcement of the fibrils. However, at the same time, the storage modulus (Figure 7a) increased monotonically with an increase of the MoS$_2$ concentration, and ultimately this overhardening led to a decrease of the tack energy (Figure 4).

The data in Figure 8 were analyzed to provide quantitative information. An enhanced stiffness can be clearly seen in Figure 9 where the Young's modulus, obtained from the stress/strain data, increases continuously with the MoS$_2$ concentration. There is also a small increase in the pseudoyield stress that accompanies the increasing modulus. The strain hardening is analyzed by plotting the maximum nominal stress (from Figure 8). The maximum stress shows an abrupt upward step between 0.1 and 0.25 wt % MoS$_2$ nanoplatelets (Figure 9b) where the strain hardening becomes evident and provides further evidence for the interactions between the platelets and the polymer. This strain hardening leads to a clean detachment of the fibrils from the substrate. Hence, it ensures adhesive failure, rather than the cohesive failure observed without MoS$_2$ present. However, the combination of a higher elastic modulus and strain hardening attributed to the MoS$_2$ at higher concentrations contributes to a decrease in the fibrillation plateau length and a corresponding decrease in the tack energy.

It is worth pointing out that, although our PU latex was synthesized by miniemulsion polymerization because it incorporates water-insoluble monomers, a similar beneficial effect of the combined use of MoS$_2$ and PVP is expected for colloidal polymers prepared by emulsion polymerization or related methods.

■ CONCLUSIONS

In this study, we have shown that the use of 2D MoS$_2$ nanoplatelets as a nanocomposite filler in PU/(meth)acrylic pressure-sensitive adhesives at very low concentrations leads to discernible adhesive and mechanical property enhancements. Aqueous dispersions of exfoliated MoS$_2$ nanoplatelets, stabilized by low molecular weight poly(vinylpyrrolidone), were blended with PU/(meth)acrylic hybrid latexes. In addition to preventing the restacking of the platelets in the dispersion, PVP acts as an interface bridge between the inorganic and polymer phases in the final film. The glass transition upward shift indicates that the nanoplatelets reduce the mobility of polymer phase. The PVP might also provide an additional energy dissipation mechanism when the MoS$_2$ slides along the interface under deformation of the nanocomposite.

The adhesive and mechanical properties of the resulting nanocomposites films were compared with those of the original PSA. The addition of a very low amount of nanoplatelets (0.1–0.25 wt %) led to a significant improvement of the PSA tack adhesion properties, as the fibrillation plateau was raised and lengthened, as the fibrils were stronger and stable in extension. A further increase of the MoS$_2$ loading resulted in a decrease of the properties, because the adhesive became too stiff and lost some dissipative properties. A superior balance of viscoelastic properties was achieved for 0.25 wt % loading of the MoS$_2$ nanoplatelets, leading to the tack adhesion energy being three times greater than that for the original PSA.

■ ASSOCIATED CONTENT

S **Supporting Information**
Detailed procedure of calculation of the Flory–Huggins interaction parameter and the critical interaction parameter for the investigated system. This material is available free of charge via the Internet at http://pubs.acs.org
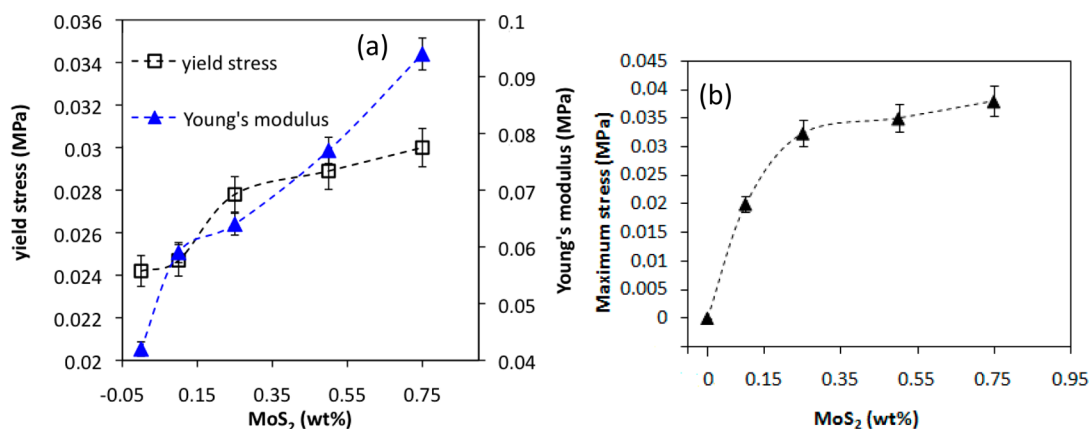
■ AUTHOR INFORMATION

Corresponding Author
*E-mail: radmila.tomovska@ehu.es.
Notes
The authors declare no competing financial interest.

Figure 9. Dependence of the bulk mechanical properties of nanocomposites as a function of MoS$_2$ concentration: (a) Young's modulus (right axis) and pseudoyield stress (left axis), and (b) maximum nominal stress in tensile tests. The dashed lines are guides to the eye.

■ REFERENCES

(1) Usuki, A.; Kojima, Y.; Okada, A.; Fukushima, Y.; Kurauchi, T.; Kamigaito, O. J. Synthesis of Nylon 6-Clay Hybrid. *Mater. Res.* **1993**, *8*, 1179−1184.

(2) Hussain, F.; Hojjati, M.; Okamoto, M.; Gorga, R. E. J. Polymer-Matrix Nanocomposites, Processing, Manufacturing, and Application: An Overview. *Compos Mater.* **2006**, *40*, 1511−1575.

(3) Godovsky, D. Y. Device Applications of Polymer-Nanocomposites. *Adv. Polym. Sci.* **2000**, *153*, 163−205.

(4) Uthirakumar, P.; Nahm, K. S.; Hahn, Y. B.; Lee, Y. S. Preparation of Polystyrene/Montmorillonite Nanocomposites Using a New Radical Initiator-Montmorillonite Hybrid Via In Situ Intercalative Polymerization. *Eur. Polym. J.* **2004**, *40*, 2437−2444.

(5) Kiersnowski, A.; Piglowski, J. Polymer-Layered Silicate Nanocomposites Based on Poly(ε-Caprolactone). *Eur. Polym. J.* **2004**, *40*, 1199−1207.

(6) Causin, V.; Marega, C.; Marigo, A.; Ferrara, G. Assessing Organo-Clay Dispersion in Polymer Layered Silicate Nanocomposites: A SAXS Approach. *Polymer* **2005**, *46*, 9533−9537.

(7) Moussaif, N.; Groeninckx, G. Nanocomposites Based on Layered Silicate and Miscible PVDF/PMMA Blends: Melt Preparation, Nanophase Morphology and Rheological Behaviour. *Polymer* **2003**, *44*, 7899−7906.

(8) Liang, Z. M.; Yin, J. Poly(etherimide)/Montmorillonite Nanocomposites Prepared by Melt Intercalation. *J. Appl. Polym. Sci.* **2003**, *90*, 1857−1863.

(9) Morgan, A. B.; Harris, J. D. Exfoliated Polystyrene-Clay Nanocomposites Synthesized by Solvent Blending with Sonication. *Polymer* **2004**, *45*, 8695−8703.

(10) Li, Y.; Ishida, H. Solution Intercalation of Polystyrene and the Comparison With Poly(ethyl methacrylate). *Polymer* **2003**, *44*, 6571−6577.

(11) Kropka, J. M.; Putz, K. W.; Pryamitsyn, V.; Ganesan, V.; Green, P. F. Origin of Dynamical Properties in PMMA−C_{60} Nanocomposites. *Macromolecules* **2007**, *40*, 5424−5432.

(12) Kajtna, J.; Sebenik, U. Microsphere Pressure Sensitive Adhesives—Acrylic Polymer/Montmorillonite Clay Nanocomposite Materials. *Int. J. Adhes. Adhes.* **2009**, *29*, 543−550.

(13) Diaconu, G.; Paulis, M.; Leiza, J. R. Towards the Synthesis of High Solids Content Waterborne Poly(methyl methacrylate-co-butyl acrylate)/ Montmorillonite Nanocomposites. *Polymer* **2008**, *49*, 2444−2454.

(14) Arzac, A.; Leal, G. P.; Fajgar, R.; Tomovska, R. Comparison of the Emulsion Mixing and In Situ Polymerization Techniques for Synthesis of Water-Borne Reduced Graphene Oxide/Polymer Composites: Advantages and Drawbacks. *Part. Part. Syst. Charact.* **2014**, *31*, 143−151.

(15) Chou, C. S.; La Fleur, E. E.; Lorah, D. P.; Slone, R. V.; Neglia, K. D. *Aqueous Nanocomposite Dispersions: Processes, Compositions, and Uses Thereof.* US 6838507 B2, 2005.

(16) Li, H.; Yang, Y. K.; Yu, Y. Z. Acrylic Emulsion Pressure-Sensitive Adhesives (PSAS) Reinforced With Layered Silicate. *J. Adhes. Sci. Technol.* **2004**, *18*, 1759−1770.

(17) Diaconu, G.; Asua, J. M.; Paulis, M.; Leiza, J. R. High-Solids Content Waterborne Polymer-Clay Nanocomposites. *Macromol. Symp.* **2007**, *259*, 305−317.

(18) Diaconu, G.; Paulis, M.; Leiza, J. R. High Solids Content Waterborne Acrylic/Montmorillonite Nanocomposites by Miniemulsion Polymerization. *Macromol. React. Eng.* **2008**, *2*, 80−89.

(19) Diaconu, G.; Micusık, M.; Bonnefond, A.; Paulis, M.; Leiza, J. R. Macroinitiator and Macromonomer Modified Montmorillonite for the Synthesis of Acrylic/MMT Nanocomposite Latexes. *Macromolecules* **2009**, *42*, 3316−3325.

(20) Micusık, M.; Bonnefond, A.; Paulis, M.; Leiza, J. R. Synthesis of Waterborne Acrylic/Clay Nanocomposites by Controlled Surface Initiation from Macroinitiator Modified Montmorillonite. *Eur. Polym. J.* **2012**, *48*, 896−905.

(21) Asua, J. M. Challenges for Industrialization of Miniemulsion Polymerization. *Prog. Polym. Sci.* **2014**, *39*, 1797−1826.

(22) Wang, T.; Lei, C. H.; Dalton, A. B.; Creton, C.; Lin, Y.; Fernando, K. A. S.; Sun, Y. P.; Manea, M.; Asua, J. M.; Keddie, J. L. Waterborne, Nanocomposite Pressure-Sensitive Adhesives with High Tack Energy, Optical Transparency, and Electrical Conductivity. *Adv. Mater.* **2006**, *18*, 2730−2734.

(23) Wang, T.; Lei, C. H.; Liu, D.; Manea, M.; Asua, J. M.; Creton, C.; Dalton, A. B.; Keddie, J. L. A Molecular Mechanism for Toughening and Strengthening Waterborne Nanocomposites. *Adv. Mater.* **2008**, *20*, 90−94.

(24) Wang, T.; Dalton, A. B.; Keddie, J. L. Importance of Molecular Friction in a Soft Polymer-Nanotube Nanocomposite. *Macromolecules* **2008**, *41*, 7656−7661.

(25) Creton, C. Pressure-Sensitive Adhesives: An Introductory Course. *MRS Bull.* **2003**, *28*, 434−439.

(26) Lindner, A.; Lestriez, B.; Mariot, S.; Creton, C.; Maevis, T.; Luhmann, B.; Brummer, R. Adhesive and Rheological Properties of Lightly Crosslinked Model Acrylic Networks. *J. Adhes.* **2006**, *82*, 267−310.

(27) Jovanovic, R.; Dube, M. A. Emulsion-Based Pressure-Sensitive Adhesives: A Review. *J. Macromol. Sci. Part C: Polym. Rev.* **2004**, *44*, 1−51.

(28) Wang, T.; Colver, P. J.; Bon, S. A. F.; Keddie, J. L. Synergistic Effects between Clay and a Soft Polymer in a Supracolloidal Structure Leading to Increased Tack Energy in Pressure-Sensitive Adhesives. *Soft Matter* **2009**, *5*, 3842−3849.

(29) Lopez, A.; Degrandi, E.; Canetta, E.; Keddie, J. L.; Creton, C.; Asua, J. M. Simultaneous Free Radical and Addition Miniemulsion Polymerization: Effect of the Diol on the Microstructure of Polyurethane-Acrylic Pressure-Sensitive Adhesives. *Polymer* **2011**, *52*, 3021−3030.

(30) Lopez, A.; Degrandi, E.; Canetta, E.; Creton, C.; Keddie, J. L.; Asua, J. M. Waterborne Polyurethane−Acrylic Hybrid Nanoparticles by Miniemulsion Polymerization: Applications in Pressure-Sensitive Adhesives. *Langmuir* **2011**, *27*, 3878−3888.

(31) Khan, U.; May, P.; Porwal, H.; Nawaz, K.; Coleman, J. N. Improved Adhesive Strength and Toughness of Polyvinyl Acetate Glue on Addition of Small Quantities of Graphene. *ACS Appl. Mater. Interfaces* **2013**, *5*, 1423−1428.

(32) Helveg, S.; Lauritsen, J. V.; Lægsgaard, E.; Stensgaard, I.; Nøskov, J. K.; Clausen, B. S.; Topsøe, H.; Besenbacher, F. Atomic-Scale Structure of Single-Layer MoS_2 Nanoclusters. *Phys. Rev. Lett.* **2000**, *84*, 951−954.

(33) Lauritsen, J. V.; Kibsgaard, J.; Helveg, S.; Topsøe, H.; Clausen, B. S.; Lægsgaard, E.; Besenbacher, F. Size-Dependent Structure of MoS_2 Nanocrystals. *Nat. Nanotechnol.* **2007**, *2*, 53−58.

(34) Novoselov, K. S.; Jiang, D.; Schedin, F.; Booth, T. J.; Khotkevich, V. V.; Morozov, S. V.; Geim, A. K. Two-Dimensional Atomic Crystals. *Proc. Natl. Acad. Sci. U.S.A.* **2005**, *102*, 10451−10453.

(35) Rapoport, L.; Nepomnyashchy, O.; Verdyan, A.; Popovitz, R.; Volonik, Y.; Ittah, B. Polymer Nanocomposites with Fullerene-like Solid Lubricant. *Adv. Eng. Mater.* **2004**, *6*, 44−48.

(36) Hou, X.; Shan, C. X.; Choy, K. L. Microstructures and Tribological Properties of PEEK-Based Nanocomposite Coatings Incorporating Inorganic Fullerene-Like Nanoparticles. *Surf. Coat. Technol.* **2008**, *202*, 2287−2291.

(37) Matusinovic, Z.; Shukla, R.; Manias, E.; Hogshead, C. G.; Wilkie, C. A. Polystyrene/Molybdenum Disulfide and Poly(methyl methacrylate)/ Molybdenum Disulfide Nanocomposites with Enhanced Thermal Stability. *Polym. Degrad. Stab.* **2012**, *97*, 2481−2486.

(38) Reinecker, M.; Fuith, A.; Soprunyuk, V.; Sánchez-Ferrer, A.; Mrzel, A.; Torre, R.; Schranz, W. Influence of Inorganic Nanoparticles on the Glass Transitions of Polyurea Elastomers. *Phys. Status Solidi A* **2013**, *210*, 2320−2327.

(39) Higuchi, W. I.; Misra, J. Physical Degradation of Emulsions via the Molecular Diffusion Route and the Possible Prevention Thereof. *J. Pharm. Sci.* **1962**, *51*, 459−466.

(40) Ugelstad, J.; Mork, P. C.; Mfutakamba, H. R. Thermodynamics of swelling of polymer olygomer and ppolymer−olygomer particles. Preparation and application of monodisperse polymer particles. In *Science and Technology of Polymer Colloids*; Poehlein, G. W., Ottewill, R. H., Goodwin, J. W., Eds.; NATO ASI Series E67; Springer: The Netherlands, 1983; pp 51−99.

(41) Daniloska, V.; Tomovska, R.; Asua, J. M. Hybrid Miniemulsion Photopolymerization in a Continuous Tubular Reactor—A Way to Expand the Characteristics of Polyurethane/Acrylics. *Chem. Eng. J.* **2012**, *184*, 308−314.

(42) Daniloska, V.; Carretero, P.; Tomovska, R.; Asua, J. M. High Performance Pressure Sensitive Adhesives by Miniemulsion Photopolymerization in a Continuous Tubular Reactor. *Polymer* **2014**, *55*, 5050−5056.

(43) Daniloska, V.; Tomovska, R.; Asua, J. M. Designing Tubular Reactors to Avoid Clogging in High Solids Miniemulsion Photopolymerization. *Chem. Eng. J.* **2013**, *222*, 136−141.

(44) Daniloska, V.; Carretero, P.; Tomovska, R.; Paulis, M.; Asua, J. M. High Performance Adhesives Resulting from Spontaneous Formation of Nanogels within Miniemulsion Particles. *ACS Appl. Mater. Interfaces* **2014**, *6*, 3559−3567.

(45) Hamzehlou, S.; Ballard, N.; Carretero, P.; Paulis, M.; Asua, J. M.; Reyes, Y.; Leiza, J. R. Mechanistic Investigation of the Simultaneous Addition and Free-Radical Polymerization in Batch Miniemulsion Droplets: Monte Carlo Simulation Versus Experimental Data in Polyurethane/Acrylic Systems. *Polymer* **2014**, *55*, 4801−4811.

(46) Wieting, T. J.; Verble, J. L. Infrared and Raman Studies of Long-Wavelength Phonons in Hexagonal MoS_2. *Phys. Rev. B* **1971**, *3*, 4286−4292.

(47) Splendiani, A.; Sun, L.; Zhang, Y.; Li, T.; Kim, J.; Chim, C. Y.; Galli, G.; Wang, F. Emerging Photoluminescence in Monolayer MoS_2. *Nano Lett.* **2010**, *10*, 1271−1275.

(48) Plechinger, G.; Heydrich, S.; Eroms, J.; Weiss, D.; Schuller, C.; Kor, T. Raman Spectroscopy of the Interlayer Shear Mode in Few-Layer MoS_2 flakes. *Appl. Phys. Lett.* **2012**, *101*, 101906−3.

(49) Zosel, A. The Effect of Fibrillation on the Tack of Pressure Sensitive Adhesives. *Int. J. Adhes. Adhes.* **1998**, *18*, 265−271.

(50) Lakrout, H.; Sergot, P.; Creton, C. Direct Observation of Cavitation and Fibrillation in a Probe Tack Experiment on Model Acrylic Pressure-Sensitive-Adhesives. *J. Adhes.* **1999**, *69*, 307−359.

(51) Lakrout, H.; Creton, C.; Ahn, D.; Shull, K. R. Influence of Molecular Features on the Tackiness of Acrylic Polymer Melts. *Macromolecules* **2001**, *34*, 7448−7458.

(52) Diethert, A.; Peykova, Y.; Willenbacher, N.; Müller-Buschbaum, P. Near-Surface Composition Profiles and the Adhesive Properties of Statistical Copolymer Films Being Model Systems of Pressure Sensitive Adhesive Films. *ACS Appl. Mater. Interfaces* **2010**, *2*, 2060−2068.

(53) Diethert, A.; Ecker, K.; Peykova, Y.; Willenbacher, N.; Müller-Buschbaum, P. Tailoring the near-Surface Composition Profiles of Pressure-Sensitive Adhesive Films and the Resulting Mechanical Properties. *ACS Appl. Mater. Interfaces* **2011**, *3*, 2012−2021.

(54) Shenoy, S. L.; Bates, W. D.; Frisch, H. L.; Wnek, G. E. Role of Chain Entanglements on Fiber Formation During Electrospinning of Polymer Solutions: Good Solvent, Non-Specific Polymer−Polymer Interaction Limit. *Polymer* **2005**, *46*, 3372−3384.

(55) Costa, A. C.; Chiche, A.; Vlcek, P.; Creton, C.; Composto, R. J. Adhesion Promotion Between a Homopolymer Probe and a Glass Substrate Coated with a Block Copolymer Monolayer. *Polymer* **2004**, *45*, 4445−4451.

(56) Dahlquist, C. A. Pressure-Sensitive Adhesives. In *Treatise on Adhesion and Adhesives*; Patrick, R. L., Ed.; Dekker,: New York, 1969; Vol. 2, pp 219−260.

(57) Deplace, F.; Carelli, C.; Mariot, S.; Retsos, H.; Chateauminois, A.; Ouzineb, K.; Creton, C. Fine Tuning the Adhesive Properties of a Soft Nanostructured Adhesive with Rheological Measurements. *J. Adhes.* **2009**, *85*, 18−54.